Constraining the entire Earth system projections for more reliable climate change adaptation planning

Chao Li, Francis W. Zwiers, Xuebin Zhang, Erich M. Fischer, Fujun Du, Jieyu Liu, Jianyu Wang, Yongxiao Liang, Tong Li, and Lina Yuan

2025

Pacific Climate Impacts Consortium (PCIC)

PCIC Publications

Original citation:
Li, C., Zwiers, F. W., Zhang, X, Fischer, E. M., Du, F, Liu, J., Wang, J., Liang, Y., & Yuan, L. (2025). Constraining the entire Earth system projections for more reliable climate change adaptation planning. *Science Advances*, *11*(9). https://doi.org/10.1126/sciadv.adr5346

CLIMATOLOGY

Constraining the entire Earth system projections for more reliable climate change adaptation planning

Chao Li[1]*, Francis W. Zwiers[2,3], Xuebin Zhang[2], Erich M. Fischer[4], Fujun Du[1], Jieyu Liu[5], Jianyu Wang[6,7], Yongxiao Liang[8], Tong Li[2], Lina Yuan[1]

The warming climate is creating increased levels of climate risk because of changes to the hazards to which human and natural systems are exposed. Projections of how those hazards will change are affected by uncertainties in the climate sensitivity of climate models, among other factors. While the level-of-global-warming approach can circumvent model climate sensitivity uncertainties in some applications, practitioners faced with specific adaptation responsibilities often find such projections difficult to use because they generally require time-oriented information. Earth system projections following specified emissions scenarios can, however, be constrained by applying the level-of-global-warming approach to observationally constrained warming projections to yield more reliable time-oriented projections for adaption planning and implementation. This approach also allows individual groups to produce consistent and comparable assessments of multifaceted climate impacts and causal mechanisms, thereby benefiting climate assessments at national and international levels that provide the science basis for adaptation action.

INTRODUCTION

Many climate models participating in phase 6 of the Coupled Model Intercomparison Project [CMIP6; (*1*)] exhibit higher climate sensitivity and transient climate response than their earlier counterparts (*2*–*5*), leading to concern about whether the CMIP6 model ensemble can be reliably used to project future climates for adaptation and resilience planning (*6*–*10*). The Intergovernmental Panel on Climate Change (IPCC) reconciled this "hot model" problem in its Sixth Assessment Working Group I report [AR6; (*11*)] by weighting models based on the consistency of their transient climate responses with multiple lines of observational evidence (*12*–*14*) as a basis for its "assessed warming" projections. This is an important advance from a global climate policy perspective because it provides reduced uncertainty on projected future warming and its timing under different scenarios (*11*), and thus greater certainty concerning the prospects for avoiding future levels of global warming above negotiated limits, such as 2°C above preindustrial levels, under a given scenario.

Setting global climate policy objectives in terms of warming limits has also led to a very large body of literature that evaluates the consequences of reaching different levels of global warming, such as 1.5°, 2°, 3°, and 4°C above preindustrial levels (*15*), and it enables those evaluations to occur in a way that circumvents climate sensitivity uncertainties in projections for different interacting variables (*11*). This is important, because the quantification of hazards and risks associated with a given level of global warming requires the consideration of multiple climate variables, compound extreme events, and the associated hazard and risk-producing mechanisms at impact-relevant spatiotemporal scales.

Nevertheless, first-hand experience of some of the authors of this paper indicates that practitioners faced with specific climate change adaptation responsibilities, such as ensuring the resilience of an electrical utility under possible future climate conditions, often find it difficult to use the level-of-global-warming approach in practice. This difficulty arises because it is necessary to determine the timing of warming, and because it becomes more difficult to quantify the uncertainty in the resulting temperature-dependent impact scenarios. In our experience, practitioners such as engineers invariably find the traditional, time-oriented approach more suitable and actionable. This is because they are charged with ensuring the resilience of a particular system over a fixed time horizon that is related to the expected service life of the system's infrastructure components, and to do so at the lowest possible cost. The characteristics of this charge lead to a need for emissions pathway specific projections for fixed future time horizons that are as robust as possible to sources of uncertainty such as climate sensitivity uncertainty and correctly reflect how the interaction between different climate variables may generate hazards affecting the system they affect.

We advance this objective with an emergent constraint approach to mitigating model-related global warming uncertainties in the time-oriented Earth system projections, using the ensemble of CMIP6 projections as an example (*1*). We do this by conditioning Earth system model projections for a scenario-based future period on observationally constrained global warming projections for that period. By leveraging the level-of-global-warming approach (*15*), such warming-constrained projections retain most of the physical processes and interactions among different components of the Earth system as resolved in models. This feature permits the development of observationally constrained time-oriented future projections that are internally consistent across the collection of variables that are needed when designing and implementing adaptation plans. This also allows individual groups to produce consistent and comparable

[1]Key Laboratory of Geographic Information Science, Ministry of Education, School of Geographic Sciences, East China Normal University, Shanghai, China. [2]Pacific Climate Impacts Consortium, University of Victoria, Victoria, BC, Canada. [3]Key Laboratory of Meteorological Disaster, Ministry of Education, Collaborative Innovation Center on Forecast and Evaluation of Meteorological Disasters, Nanjing University of Information Science & Technology, Nanjing, China. [4]Institute for Atmospheric and Climate Science, ETH Zurich, Zurich, Switzerland. [5]College of Atmospheric Sciences, Lanzhou University, Lanzhou, China. [6]State Key Laboratory of Severe Weather, Chinese Academy of Meteorological Sciences, Beijing, China. [7]University of Chinese Academy of Sciences, Beijing, China. [8]Climate Research Division, Environment and Climate Change Canada, Victoria, BC, Canada.
*Corresponding author. Email: cli@geo.ecnu.edu.cn

assessments of different dimensions of the Earth system, thus benefiting a more integrated science basis for climate adaptation.

RESULTS

An emergent constraint strategy for the entire Earth system projections

The proposed constraint strategy for Earth system projections for a future period involves two steps. We first use an established emergent constraint method (*16*) to derive future global warming projections relative to preindustrial 1850 to 1900 constrained by the observed warming of global mean near-surface air temperature during 1971 to 2020 (Materials and Methods). Basically, the method regards the collection of raw global warming projections for a given future period as a prior distribution p_1 and then uses a simple hierarchical Bayesian statistical approach to obtain a posterior projected warming distribution p_2 that is conditional on the observed warming. The posterior distribution p_2, which describes the projected warming for the given future period constrained by (that is, conditional on) the observed warming, turns out to be a very good emulator of the IPCC-assessed warming projections (fig. S1A). In practice, one can also adopt the IPCC's approach to obtain a posterior distribution p_2 (*11*). The effect of conditioning the warming projections on the observed warming is to shift the distribution of projected warming amounts to somewhat lower levels compared to the raw model projections and to narrow the distribution (fig. S1B), thereby reducing the influence of the models with the highest climate sensitivities such as the so-called hot models. Second, we use the posterior distribution of the warming for the future period p_2, or equivalently the corresponding warming assessed by the IPCC, to constrain projections of the entire Earth system for that period.

As illustrated schematically in Fig. 1, the raw warming projections from individual climate models for a particular projection period are used to estimate a prior distribution p_1, which is then updated using the observed 1971 to 2020 warming trend to obtain an observationally constrained posterior projected warming distribution p_2 for that period (Fig. 1, top left). The raw warming projections are then mapped to a set of constrained projections conforming with p_2 via quantile mapping, producing one constrained warming projection for each model (fig. S2 for an illustration of the quantile mapping process;

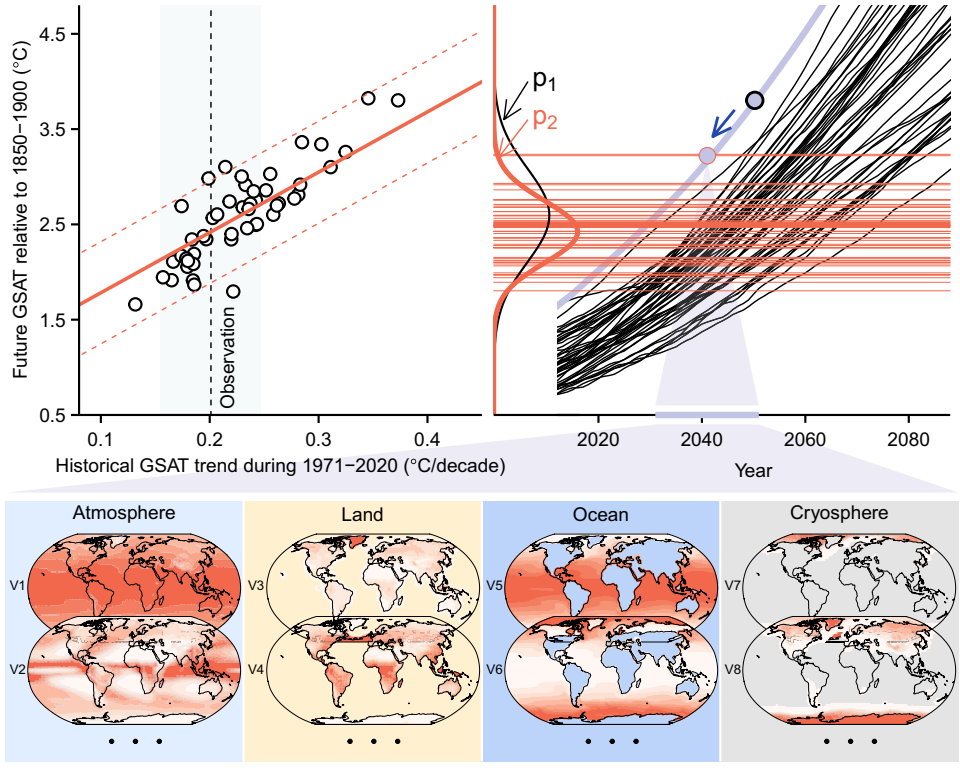

Fig. 1. A schematic illustration of the constrained level-of-global-warming approach. An emergent constraint method using the observed warming during 1971 to 2020 as an observational constraint is adopted to derive a constrained distribution for future warming (by mid-term 2041 to 2060 under the SSP5-8.5 emissions scenario; top left). The unconstrained warming projections from individual climate models conforming with distribution p_1 are converted to a set of warming projections conforming with the constrained warming distribution p_2 through quantile mapping (see fig. S2 for an illustration). The constrained warming projections are then used to identify 20-year windows (the same length as the 2041 to 2060 projection period) when models warm to their constrained warming projections; for example, the blue arrow indicates that the projection period 2041 to 2060 in CanESM5 is updated to 2031 to 2050 according to its constrained warming projection (top right). The Earth system projections in the identified model time windows (e.g., 2031 to 2050 rather than 2041 to 2060 for CanESM5) are considered as the observed warming-constrained projections (bottom; e.g., illustrated in the maps are the long-term means of the 2031 to 2050 projections of atmosphere variables of annual mean temperature and precipitation, land variables of soil moisture content and evapotranspiration, ocean variables of sea surface temperature and dissolved oxygen, and cryosphere variables of sea ice concentration and snow concentration from CanESM5).

Materials and Methods). For each model, we then identify the time window in which the constrained projected warming for that model occurs (Fig. 1, top right). We consider its simulation of the Earth system in that time window as its observed warming-constrained Earth system projection for the period of interest (Fig. 1, bottom). A key feature of this approach is that the constrained Earth system projections are globally consistent with the observationally constrained global warming, while the relationships between Earth system variables are unaltered within individual model simulations. In addition, changes in these relationships are affected by similar amounts of global warming for all models. These two factors together ensure that it remains possible to comprehensively study different dimensions of the Earth system using internally consistent variables and metrics.

Merits of jointly constraining time-oriented Earth system projections

First and foremost, the strategy allows users to approach impacts and adaptation challenges in a traditional, sequential fashion, starting with the identification of a time horizon of interest, then assessing how much warming will take place by that time under an assumed emissions scenario, and finally determining corresponding impacts and adaptation measures to mitigate the risks that would materialize. The strategy also enables the development of storylines for climate change impacts by allowing the investigation of their causal mechanisms and compounding and/or cascading impacts with other changes. Properly formulated storylines describing the future climate can help adaptation practitioners and stakeholders understand how hazards and risks materialize (*17*, *18*). In contrast, observational constraint strategies (*12*–*14*, *19*–*27*) that are implemented separately on individual Earth system variables may obscure the interactions among variables and thus impede the process of understanding hazard development mechanisms.

Moreover, the strategy enables individual groups to produce consistent and comparable assessments of climate change impacts through consistent treatment of models contributing to a given ensemble of future climate projections. This would help to enhance the integration of assessments by contributing to the coherent cumulation of knowledge about projected climate change impacts. To facilitate that, we have deployed an interactive online tool for identifying the time windows for the constrained projections for different CMIP6 models, emissions scenarios, and future periods (https://ecop-earth.com). Individual groups can use Earth system simulations in these time windows to perform assessments of different dimensions of climate change impacts without the need for extensive coordination efforts. This would greatly benefit both national climate scenarios and international climate assessments, which provide the science basis for climate adaptation, such as the next IPCC assessment cycle.

In contrast to previous suggestions (*6*, *8*–*10*), "hot" or "cool" models are not mandatorily excluded. By adjusting effective projection periods in accordance with the constrained global warming, the constrained projections integrate evidence from all available Earth system models. Arguably, there is no established reason to exclude either hot or cool models from the projections for variables that are generally not sensitive to global warming but necessary for understanding the causal mechanisms of changes in variables depending strongly on warming, such as atmospheric circulation features favorable to precipitation and climate extremes (*21*, *25*, *28*, *29*), as will be demonstrated. The approach is also more attractive than model weighting strategies (*9*, *13*, *30*, *31*) because weighted averaging may result in physically unrealistic projections for nonlinear processes and interactions.

Additional observational constraints can flexibly be imposed on the conditional Earth system projections when appropriate. For example, observational constraints that have been proposed for global hydrologic sensitivity (*32*, *33*) and Arctic amplification (*22*, *34*) can be applied in a second step after constraining the full Earth system projections to further improve their reliability, as will be illustrated in the following subsection. In addition, many applications, such as sectoral impact studies, require additional bias correction to avoid the effects of systematic climate model biases on impact model performance (*35*, *36*). This type of model output postprocessing, which deals with absolute level biases in climate variables rather than biases in their changes associated with warming projections, benefits substantially from the narrowing of projection uncertainty that is achieved by first constraining Earth system projections as we have proposed.

Effectiveness evaluation

A model-based evaluation is conducted to assess the effectiveness of the suggested constrained level-of-global-warming approach in mitigating hot model influences (*21*). As hot models manifest directly in temperature projections, we focus on the projected changes in annual mean near-surface air temperature at model grid cell to global scales. We divide models into two groups according to their equilibrium climate sensitivities [table S1; (*4*)]: one group consisting of 10 "cool" models with the lowest climate sensitivities among models considered and the other group consisting of the remaining models, which, for simplicity, are referred to as hot models. While we only have observations of the past, models provide realizations of the past climate and continuing realizations of the future climate that can stand in for observations when testing the performance of constraint schemes. We therefore use each cool model in turn to provide such "pseudo observations" of the past and future and assess whether projections of future temperature changes made with the hot models that are constrained by the past warming in the pseudo observations indeed provide better estimates of the future warming in those pseudo observations. A paired *t* test at the 5% significance level is used to ascertain whether the constrained warming projections are significantly less biased or uncertain compared to the unconditioned projections.

Figure 2 contrasts the biases in the constrained and unconstrained projections of annual mean near-surface air temperatures averaged over the globe and at model grid cells for mid-term (2041 to 2060) and long-term (2071 to 2090) future periods under moderate and high emissions scenarios as designated by the Shared Socioeconomic Pathway 2-4.5 (SSP2-4.5) and SSP5-8.5 (*37*), respectively. See table S1 for information about the models and simulations considered. Warm biases remain in the constrained projections but are significantly smaller than those of the unconstrained hot model projections at the 5% level (see fig. S3 for the relative biases). In addition, the constrained projections are significantly less uncertain than unconstrained projections at the 5% level across the planet (fig. S4). On average over the globe and across the considered projection periods and emissions scenarios, the percentage reductions in bias and error variance are 40 and 43%, respectively. Projections with reduced warming bias and uncertainty are expected to also project more reliable changes in other Earth system variables and processes, especially those dominated by thermodynamic responses.

We notice that the remaining hot biases are notable in the Arctic region (i.e., north of 65°N; Fig. 2C). The Arctic warming amplification

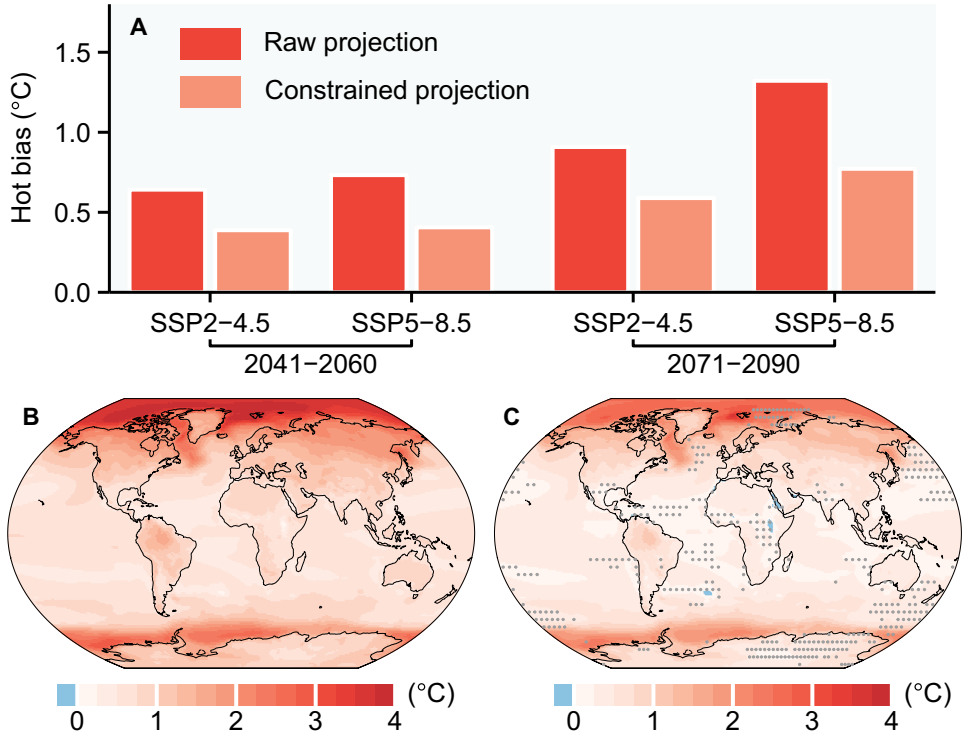

Fig. 2. Model-based evaluation of the constrained level-of-global-warming approach in reducing warming bias. (**A**) Biases in the estimated changes in annual global mean near-surface air temperature by 2041 to 2060 and 2071 to 2090 under SSP2-4.5 and SSP5-8.5 scenarios in cool models using hot models with and without applying the constrained level-of-global-warming approach. (**B**) Spatial pattern of bias of hot model unconstrained projections when considered as estimates of warming in cool models, averaged across both projection periods and both emissions scenarios. (**C**) As (B), except comparing hot model constrained level-of-global-warming projections to estimate cool model warming. Stippling in (C) indicates locations where the constrained level-of-global-warming approach does not significantly reduce bias at the 5% level in one or more of the four considered scenario periods. The stippled grid cells amount to 20% of the total grid cells, which is substantially less than the fraction that would be expected to be stippled (~82%) if the constraint were ineffective in reducing bias in all considered projection periods.

due to regional processes such as surface albedo feedback, as measured by the sensitivity of Arctic temperature to global warming, is not strongly related to global climate sensitivity [fig. S5A; (*22*, *34*)]. The weak relationship between Arctic amplification strength and model equilibrium climate sensitivity makes it challenging to estimate Arctic warming in "cool models" using hot models in terms of a single global temperature constraint, and vice versa. This is in line with the reported weaker global temperature constraint for Arctic warming (*38*) than for global warming (*12*). Similar challenges exist in regions affected by strong regional external forcings and feedback processes. Nevertheless, applying additional observational constraints to the globally constrained projections for specific regions can further reduce biases and uncertainties related to these regional processes. For example, the globally constrained multimodel projections of future Arctic warming show strong correlations with the strength of Arctic amplification in these models (estimated as well from the constrained global projections; fig. S5B). Thus, observational constraints for the amplification strength (*34*) can be used as additional constraints to mitigate remaining biases and uncertainties in Arctic warming projections caused by regional climate sensitivity uncertainties, but possibly at the expense of losing physical consistency with other variables.

In addition, it should be noted that using hot models to project changes in cool models provides a stringent stress test for the constraint strategy. Practical applications would use the full set of available models to project the most likely future climate rather than just the hot models. Moreover, it is unlikely that the discrepancy between the median climate sensitivity of the full set of models and that of the observed world is as large as the discrepancy in sensitivity between the hot and cool models.

Constrained future climate extremes

We apply the constrained level-of-global-warming approach to assess the time-oriented projections of future changes in temperature and precipitation extremes under the high SSP5-8.5 and the moderate SSP2-4.5 emissions scenarios. We focus primarily on the high SSP5-8.5 scenario because the hot model effects intensify with stronger external forcings, and this high-end emissions scenario is particularly useful for assessing the potential severe stress that infrastructure may face in the future due to climate extremes. We consider changes in annual maximum temperature (TXx) and annual maximum daily precipitation (Rx1day). Daily output suitable for calculating both TXx and Rx1day is available for 20 Earth system models (table S2). In contrast, much more models provide output suitable for developing a warming constraint (48 models under SSP5-8.5 and 46 models under SSP2-4.5; table S1), which we use to constrain the 20 models with TXx and Rx1day. Using all available models to develop the warming constraint ensures that it is as representative as possible of current Earth system models and facilitates intercomparations of assessments for variables archived by different subsets of the CMIP6 models.

The constrained projections under the SSP5-8.5 emissions scenario obtained using the observed 1971 to 2020 global mean near-surface air temperature trend in HadCRUT5 (*39*) indicate more moderate changes to both temperature and precipitation extremes than unconstrained projections (Fig. 3). By late this century (2071 to 2090), the typical hottest day in the year over land would be 4.8°C hotter (2.1° to 6.8°C for the 5 to 95% spatial range) relative to preindustrial 1850 to 1900 (Fig. 3A), which is about 0.23°C cooler than expected from raw model projections (Fig. 3B). The typical wettest day in the year over land is projected to become 32% (10 to 59%) wetter than preindustrial, with a few exceptions in very limited subtropical oceans (Fig. 3C). On average, the constrained intensification of Rx1day over land is about 95% of the unconstrained rate (87 to 102%; Fig. 3D). In addition, we find that the scaling of Rx1day changes with respect to global warming is almost the same after constraint as it is in the raw projections, confirming that the constraint retains causal relations affecting extreme precipitation changes in climate models (fig. S6).

For both variables, the upper bound of the range of raw projections is reduced more strongly than the lower bound (fig. S7, A and C), leading to material reductions in the variance of the constrained projections (fig. S7, B and D), with a global land average reduction of 22% for temperature extremes and 18% for precipitation extremes. This has important climate adaptation policy implications given that the cost of implementing adaptation policy is dominated by the upper tail of projected changes in extremes. Note that the variance reductions for precipitation extremes are spatially variable and even negative in a few grid cells (fig. S7D), primarily due to the high natural variability of extreme precipitation (*40*–*42*) and the differing impacts of circulation changes across models (*43*–*45*). The influence of internal variability under the moderate SSP2-4.5 scenario is substantial enough to produce considerable areas with increased constrained changes (fig. S8D) and error variance (fig. S9D) for extreme precipitation. Given that the CMIP6 climate models generally project higher warming than indicated by observational evidence (*2*–*5*), the constrained level-of-global-warming approach effectively shifts the target projection period to earlier model timelines with comparatively weaker external forcing. As a result, the relative role of internal variability may increase, potentially obscuring the forced extreme precipitation changes under low emissions scenarios after applying the constraint. However, when internal variability is reduced, for example, at regional or larger scales, the constraint strategy effectively reduces projection uncertainties for extreme precipitation across most IPCC regions [fig. S10; (*46*)].

Constrained emergence of new normals for future climate extremes

While curbed, the constrained changes in temperature and precipitation extremes are still substantial, and thus, it is natural to ask whether a historical extreme event will become a normal event in the coming decades, and if so, when? These questions are particularly relevant for assessing the time left for adaptation (*47*–*49*) and the resilience of an infrastructure system over its design life. As an example, we consider when rare 50-year TXx and Rx1day events (i.e., 98th percentile) in the present-day (1951 to 2020) climate become relatively common 5-year (i.e., 80th percentile) events in the future climate, considering moving 20-year windows from 2021 to 2040, to 2071 to

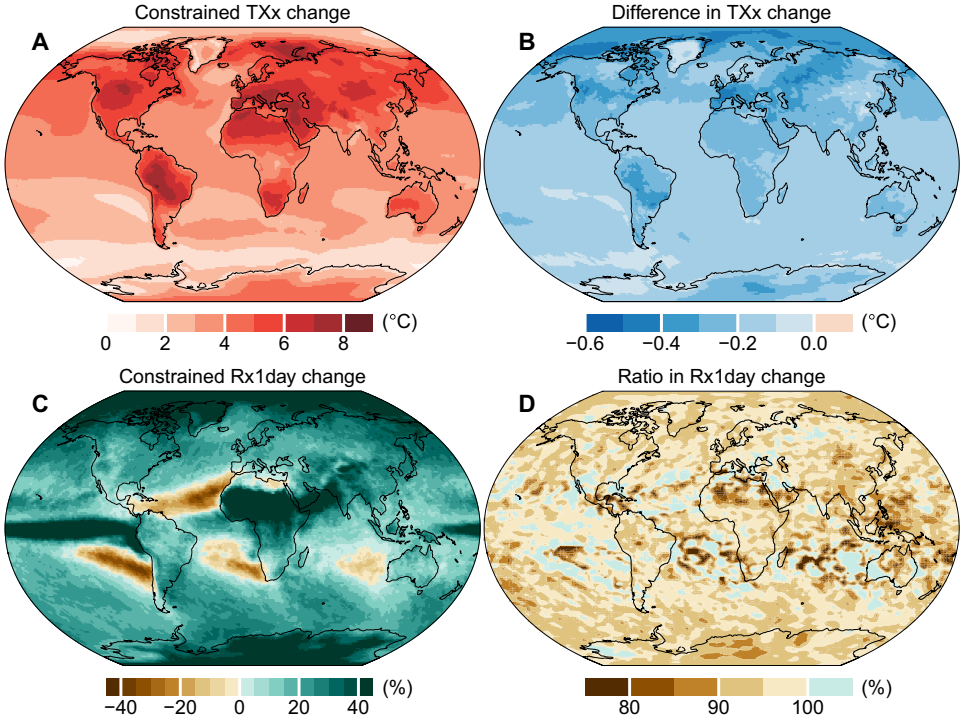

Fig. 3. Constrained future changes in temperature and precipitation extremes. Projected multimodel ensemble mean changes in annual maximum daily temperature [TXx (**A**)] and precipitation [Rx1day (**C**)] during the SSP5-8.5 scenario period of 2071 to 2090 relative to 1850 to 1900 by the constrained level-of-global-warming approach, and their differences with respect to unconstrained projections (**B** and **D**). The differences for Rx1day changes are expressed as percentage ratios of the constrained changes relative to unconstrained changes. Results for the SSP2-4.5 scenario are shown in fig. S8.

2090, as defined for projection periods in IPCC AR6 (*11*). For each model, we define the 10th year of the first window in which the historical 50-year events become 5-year events as the time at which the historical extreme event emerges as a normal event in that model. We take the multimodel median time at grid cells if the detected emergence is earlier than 2075 in more than 80% of models to ensure that the emergence persists for more than 5 years in most models. Using 30-year moving windows produces qualitatively similar emergence detection, but with slightly earlier and more widespread emergence due to reduced internal variability over longer periods.

The constrained projections suggest that historical 50-year heat events will become relatively common 5-year events over 88% of the globe by late this century (2071 to 2090) under the SSP5-8.5 scenario (Fig. 4A), covering 94% of the inhabited land area based on the 2020 global population distribution (*50*). These extreme heat events are projected to emerge as "normal" 5-year events within the next decade or so over the low-latitude oceans and arid land areas and to emerge as biennial or more frequent events over these areas within this century (Fig. 4B). The moderate SSP2-4.5 emissions scenario would still leave these regions vulnerable to such exposure (fig. S11). The notably earlier emergence at low latitudes is consistent with the much higher rate of the warming in TXx relative to its year-to-year variation in these regions [fig. S12; (*51*–*53*)].

The constrained emergence date for heat extremes tends to be 2 to 8 years later than in unconstrainted projections, but exhibits no notable difference for the very early transition of 50-year events into normal 5-year events over the Amazon, the desert areas of Africa and the Arabian Peninsula, and broad ocean areas under both emissions scenarios considered (Fig. 4C and fig. S11C). Uncertainties in emergence time projections are not reduced because the linear correlation between the emergence metric and global warming is weak (not shown). Owing to the substantially larger influence of internal variability, we did not detect local emergence for such changes in Rx1day. Nevertheless, the historical 50-year Rx1day events would become two or more times as likely in parts of the high latitudes and deep tropics within the century based on the constrained SSP5-8.5 projections (fig. S13).

Mechanisms of constrained future climate extremes

The entire Earth system constraint strategy makes it possible to also investigate the physical underpinnings of these constrained extreme temperature and precipitation changes. Such investigations require multiple variables that must be internally consistent both among themselves and with the constrained changes. For example, the constrained Rx1day changes can be decomposed into thermodynamic contributions from changes in atmospheric water vapor and dynamic contributions from changes in upward air motion using, for example, a physical diagnostic for extreme precipitation [Materials and Methods; (*44*, *45*)] and the corresponding diagnostic variables where all variables are constrained through the entire Earth system strategy, ensuring internally consistency. Doing this reveals that the projected widespread intensification of Rx1day results mainly from atmospheric water vapor increases caused by warming (fig. S14A), while the subtropical weakening of Rx1day is mainly due to a reduction of upward air motion at the time of extreme precipitation (fig. S14B). These results are consistent with previous findings using raw, unconstrained projections from the fifth phase of CMIP models (*45*), highlighting the advantage of the entire Earth system constraint strategy in generating internally consistent projections for all Earth system variables.

DISCUSSION

Although simple, our case study clearly illustrates the flexibility of the constraint strategy in synthesizing climate change impacts on different variables, changing attributes, and underlying mechanisms to develop a time-oriented tractable combined assessment that maintains physical relationships among the assessed dimensions as well as their consistency with observational evidence on the response of global warming to greenhouse gas increases. Maintaining physical consistency at

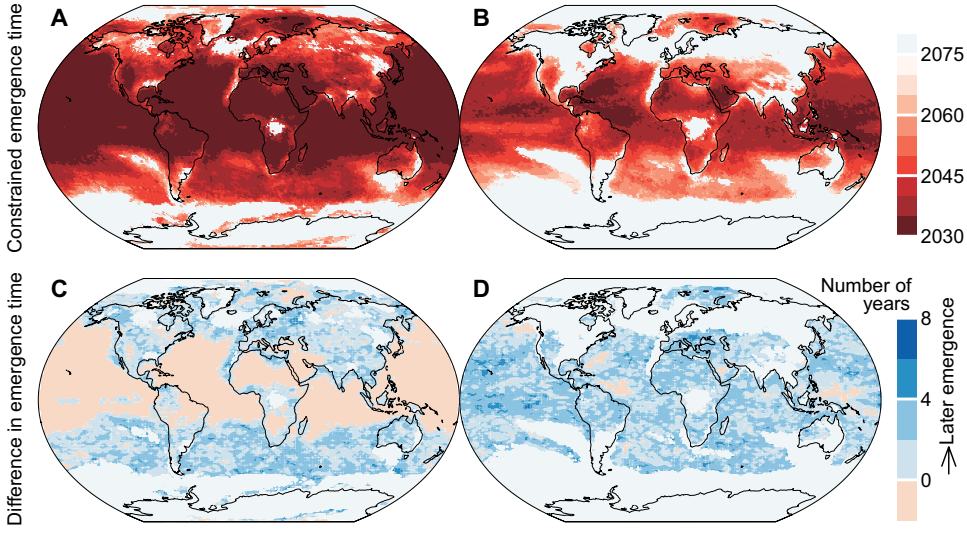

Fig. 4. Constrained time when the present-day extreme temperature event becomes a normal event. Panels show the projected multimodel ensemble median time when the 50-year extreme annual maximum temperature event during the present-day (1951 to 2020) climate would become a normal 5-year event (**A**) or a 2-year event (**B**) under the SSP5-8.5 emissions scenario, as estimated by the constrained level-of-global-warming approach (A), as well as the differences compared to the time estimates from unconstrained projections (**C** and **D**). Results for the SSP2-4.5 scenario are shown in fig. S11.

different locations, times, and for different variables is particularly important when the constrained projections are used to drive impact models, such as crop, hydrologic, or economic models (*54*–*56*), which are often used to determine how projected climate change translates into hazards and risks in different sectors, thereby helping to support effective adaptation, management, and decision-making.

The IPCC AR6 has concluded that every additional increment of global warming would cause more frequent and more intense impacts of changes in various climate extremes (*11*). Countries and communities urgently need to devote adaptation efforts to safeguard people and nature, which require guidance with a state-of-the-art science basis. The level of global warming for assessing projected impacts cannot effectively serve adaptation planning and implementation given the fact that assessing, planning, and monitoring adaptation measures nearly always needs time-oriented projections of future climate change. Our strategy represents a practical solution to bridge this gap between climate science and adaptation practice. The observationally constrained internally consistent entire Earth system projections at grid cell scales for user-defined time horizons will materially help adaptation policymakers and practitioners make informed decisions and avoid maladaptation. Combining the strategy and the IPCC-assessed warming will also mitigate concern about the potential inconsistency of time-oriented projections with the assessed warming. While the strategy primarily mitigates model-related warming uncertainties and cannot serve as a universally effective constraint for all climate elements, Earth system variables, and regions, additional constraints can be applied to the constrained projections when appropriate, as we have demonstrated for Arctic warming projections.

We have used the warming observed during 1971 to 2020 as an observational constraint on future warming. In contrast to many previous studies (*12*, *13*, *19*, *23*, *38*, *57*, *58*), our constraint includes observations and simulations of longer period to reduce internal variability uncertainties in the estimates of past warming trends in both observations and simulations. During this extended period, the greenhouse gas forcing changes fall at the upper edge of the changes during all 50-year segments since preindustrial, while the global aerosol radiative forcing changes are close to zero [fig. S15; (*59*)]. A rigorous detection and attribution analysis (*60*, *61*) confirms that the warming observed in this period was dominated by increasing greenhouse gases, while the fingerprints of forcing agents other than greenhouse gases are not detectable (Fig. 5; Materials and Methods). These results suggest a strong physical basis for using the 1971 to 2020 warming trend to constrain future climate changes driven similarly by greenhouse gas increases.

Sea surface warming patterns have been discussed as an important source of uncertainty in global warming and climate impact projections (*62*–*68*). This pattern effect is assumed to influence the projections in two ways. First, the observed sea surface temperature trends, particularly during 1981 to 2014, exhibit strong warming in the western tropical Pacific Ocean and cooling in the eastern Pacific and Southern Oceans, while CMIP6 climate models generally simulate a more uniform warming during this period (*66*–*68*). It has been argued that this may undermine the use of the 1981 to 2014 warming trend to constrain future projections (*66*). In contrast, the observed sea surface temperature warming-cooling contrast is weak when considering the longer 1971 to 2020 period (fig. S16A). The pattern of strong warming in the western tropical Pacific Ocean and cooling in the eastern Pacific and Southern Oceans seen during 1981 to 2014 may be explained as a mode of multidecadal internal variability in the 1971 to 2020 period (fig. S16, C and D) and is estimated to have minimal influence on observed global warming over this longer period, falling well within the range of internal variability as suggested by preindustrial control simulations (fig. S16E). These findings, together with our fingerprinting analysis of external drivers behind the observed warming over 1971 to 2020, enhance confidence in our constrained Earth system projections. On the other hand, sea surface temperature warming patterns can evolve

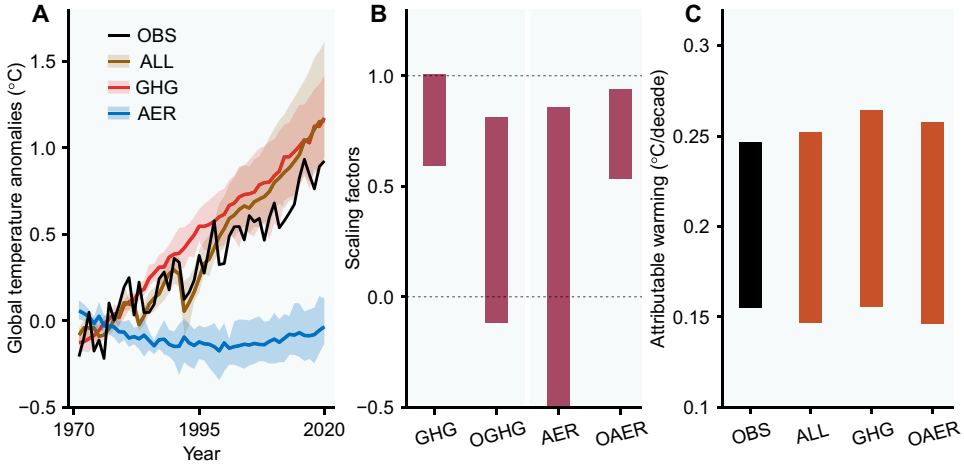

Fig. 5. Fingerprinting of the dominant forcings of the observational constraint. (**A**) Time series of 5-year running mean anomalies of global mean near-surface air temperature during 1971 to 2020 relative to 1961 to 1990 in HadCRUT5 (black) and the CMIP6 model simulations driven by historical all-known forcings (brown), greenhouse gases changes (red), and aerosol changes (blue). Shading and colored lines represent the ranges and averages of the ensemble mean anomalies from individual models. (**B**) The 90% uncertainty ranges of scaling factors for forcings from greenhouse gases (GHG) and other agents than greenhouse gases (OGHG) and for forcings from aerosols (AER) and other agents than aerosols (OAER) estimated from two-signal optimal fingerprinting analysis. (**C**) The best estimates and 90% uncertainty ranges of the observed warming over 1971 to 2020 in HadCRUT5 due to internal climate variability uncertainty (OBS) and the warming attributable to all-known historical forcings (ALL), GHG, and OAER forcings. See details of the fingerprinting analysis in Materials and Methods.

differently in different climate models, influencing warming and climate impact projections (*62*–*65*). Our global constraint strategy retains the sea surface temperature patterns and associated influences as projected in the models.

Despite the different lines of evidence and substantial effort and progress in developing observational constraints on equilibrium and transient climate sensitivities and future global warming, our understanding of the factors that influence the climate sensitivity of Earth system models remains immature (*2*–*5*, *62*–*68*). Tracking down the causes of the spread in model climate sensitivity and identifying optimal observational constraints is thus an active research field (*2*, *4*, *5*, *67*, *68*). Along with future progress in the development of more efficient observational constraints, the suggested entire Earth system constraint strategy is expected to further improve reliability and usability of Earth system model projections to accelerate adaptation across the world.

MATERIALS AND METHODS

The observed past warming and pattern effect

Estimates of the 1971 to 2020 global warming trend differ by <0.01°C per decade among different global temperature datasets (*39*, *69*–*71*). We therefore chose to use the warming in HadCRUT5 [spatially infilled version; (*39*)] as an observational constraint on future warming because its trend is close to the mean value of the available datasets (*11*). The estimated global warming during 1971 to 2020 is 0.2°C per decade. We use the standard deviation of warming estimates from a set of 50-year segments of Earth system model simulations for preindustrial climates to represent the uncertainty in this trend due to internal climate variability, which we find to be 0.03°C per decade.

Recent studies suggest that using the past warming trend, particularly during 1981 to 2014, to constrain future warming may lead to conservative projections if not accounting for the pattern effect of sea surface temperature changes (*66*–*68*). To investigate the pattern effect on the observed warming during the extended period 1971 to 2020, we conducted an empirical orthogonal function analysis on the annual mean sea surface temperature fields for this period using data from the Extended Reconstructed Sea Surface Temperature version 5 [ERSSTv5; (*72*)]. We found that the second empirical orthogonal function is characterized by warming in the western tropical Pacific Ocean and cooling in the eastern Pacific and Southern Oceans (fig. S16C), a pattern that has been widely discussed for its role in reducing the observed global warming (*66*–*68*). The associated principal component suggests that this pattern primarily manifests as multidecadal internal variability during the extended period 1971 to 2020 (fig. S16D). Regressing the observed global warming onto this principal component reveals only minimal influence of the pattern effect on the observed warming during 1971 to 2020 (fig. S16E), though the estimate may vary slightly depending on the choice of estimation methods (*71*).

To further pinpoint underlying drivers of the observed warming, we conducted an optimal fingerprinting analysis (see the following section for details). The results reveal that anthropogenic greenhouse gas increases have contributed a global warming of 0.19°C per decade over 1971 to 2020 with a 5 to 95% range of 0.12° to 0.26°C per decade, while the combined natural and anthropogenic forcings have contributed a global warming ranging from 0.14° to 0.27°C per decade (Fig. 5). These ranges are consistent with the range of the observed warming due to internal climate variability, that is, 0.15° to 0.25°C per decade.

Moreover, we note that the hierarchical emergent constraint method (*16*) used in our strategy suitably accounts for the observational uncertainty arising from internal climate variability in the calculation of the posterior distribution of the constrained warming projections; that is, the observational uncertainty is reflected in the constrained warming projections.

Fingerprinting analysis of the observed warming

The physical basis for using the observed warming during 1971 to 2020 to constrain future warming is justified if the observed warming is driven mainly by atmospheric greenhouse gas increases. We regress the nonoverlapping 5-year means of observed global mean near-surface air temperature anomalies in HadCRUT5 [relative to 1961 to 1990; (*39*)] T_o onto the corresponding simulations from Earth system models driven by specified external forcing agents T_m

$$T_o = \beta\left(T_m + \varepsilon_m\right) + \varepsilon_o \quad (1)$$

where ε_o represents internal variability in the observations T_o and ε_m represents internal variability in T_m. We estimate the scaling factors β using a regularized total least-squares approach (*59*, *60*). The fingerprinting analysis is performed using six Earth system models that have three or more simulations for 1971 to 2020 under the considered external forcing agents [(*37*, *73*); table S3].

We consider two regression configurations to pinpoint the dominating drivers for the warming observed during 1971 to 2020. The first configuration involves model simulations that are driven by all-known historical forcings and greenhouse gases forcing only, respectively. We estimate the scaling factors for fingerprints of greenhouse gases forcing and forcings other than greenhouse gases with this configuration. The second configuration includes simulations under all-known historical forcings and aerosol forcing only, respectively. This configuration provides us with scaling factors for the fingerprints of aerosol forcing and forcings other than aerosols. Fingerprints of external forcing agents are considered to have been detected in the observations if the corresponding scaling factors are greater than zero at the 5% significance level.

We estimate the amounts of global warming over 1971 to 2020 that are attributable to different forcing agents by the optimal fingerprinting analysis. The amount of warming attributable to anthropogenic greenhouse gas increases and that to forcings other than aerosols are estimated using the above two regression configurations, respectively. In addition, we estimate the amount of warming induced by all-known forcings by an optimal fingerprinting regression that only considers all-forcing historical simulations.

The strategy for conditioning future earth projections on constrained warming

Given a set of simulated warming trends for the historical period 1971 to 2020 and projected warming amounts for a scenario-specific future period relative to preindustrial 1850 to 1900 from an ensemble of CMIP6 Earth system models, we use a hierarchical emergent constraint method (*16*) to obtain a distribution p_2 for future warming that is constrained by the observed warming as follows

$$p_2\left[\mu_F + \frac{\rho\sigma_F\sigma_H}{\sigma_H^2+\sigma_{H\_obs}^2}\left(\mu_{H\_obs}-\mu_H\right), \sigma_F^2\left(1-\frac{\rho^2}{1+\sigma_{H\_obs}^2/\sigma_H^2}\right)\right] \quad (2)$$

where $p_2(\cdot)$ denotes the normal cumulative distribution function with mean and variance given by the two terms in the outer brackets, ρ is the correlation between the historical warming trends and future warming amounts in Earth system models, μ_F and σ_F are the ensemble mean and standard deviation of the projected future warming amounts, μ_H and σ_H are the corresponding values of the simulated historical warming trends, and μ_{H_obs} and σ_{H_obs} denote the observed warming trend and associated internal warming variability. It should be noted that while there is no technical limitation on how different the posterior distribution can be from the prior distribution, a large shift of the distribution beyond the range of the models would lead to very low confidence in the ability of the models to simulate historical trends in global mean surface temperature, and thus seriously compromise the physical basis for applying the constraint.

Denoting the cumulative distribution function for the raw warming projections by $p_1\left(\mu_F, \sigma_F^2\right)$, we convert the raw projections to a set of constrained projections conforming to the distribution p_2 by quantile mapping (see fig. S2 for a schematic illustration)

$$\delta T_i \rightarrow p_2^{-1}\left[p_1\left(\delta T_i\right)\right] \tag{3}$$

where δT_i is the projected warming by model i and $p_2^{-1}(\cdot)$ is the inverse (quantile) function of $p_2(\cdot)$. Model time windows when models warm to their corresponding constrained warming projections can be identified from their raw output. Although the identified time windows depend to some extent on the window width, we consider 20-year windows for consistency with the length of commonly used projection periods, such as those in the IPCC AR6. The Earth system projections in the identified time windows can be analyzed to assess climate change impacts from multiple dimensions. We consider 2071 to 2090 as the last projection window to ensure that all the models considered can reach their corresponding constrained warming projections in the available simulations that mostly end in the year 2100.

To obtain emergent constraint relationships for future warming that are as representative as possible of the CMIP6 cohort of Earth system models, we use all Earth system models providing necessary simulations to calculate global mean near-surface air temperature for the period 1850 to 2100. There are 48 such models for SSP5-8.5 emissions scenario simulations and 46 models for SSP2-4.5 scenario (table S1). Emissions scenarios SSP1-2.6 and SSP3-7.0 are also included in the interactive online tool (https://ecop-earth.com). For each climate model, we average available simulations to reduce the influence of internal variability on the estimated warming. Overall, the composition of the Earth system model ensemble does not notably affect the constrained warming projections (fig. S17).

Assessing changes in climate extremes

We analyze annual maximum daily maximum temperature and daily precipitation for the period 1850 to 2100 as simulated in 20 Earth system models that provide the necessary daily output (i.e., merged historical simulations and SSP5-8.5 or SSP2-4.5 scenario projections with daily surface air temperature and precipitation output; table S2). All annual maximum values are bilinearly interpolated to a common 1° × 1° grid to facilitate multimodel ensemble analysis. Note that we derive the conditional warming projections and adjusted projection periods for these 20 models using all available models that provide necessary simulations for calculating global mean near-surface air temperatures, as explained above.

We first analyze future changes in the two extreme variables relative to the preindustrial period 1850 to 1900. We then ask the question of whether these changes would lead to future conditions under which historical (1951 to 2020) rare extreme events (50-year events) become normal events with recurrence times of no more than 5 or 2 years, and if so, project when this would happen. To that end, we compare the intensity of historical rare 50-year events and the intensity of normal events in the future climate, considering moving 20-year windows from 2021 to 2040, to 2071 to 2090. We define the 10th year of the first window in which the historical 50-year events become as normal events in intensity as the time at which the historical event emerges as a normal event.

We analyze the physical mechanisms driving the constrained changes in annual maximum daily precipitation by diagnosing their thermodynamic contributions from changes in atmospheric water vapor and dynamic contributions from changes in atmospheric vertical velocity, using the constrained, internally consistent projections of necessary variables. According to a physical scaling diagnostic for extreme precipitation (*44*), changes in annual maximum daily precipitation between two periods can be approximated as

$$\Delta\overline{P} \approx \Delta\overline{P_s} = \frac{1}{g}\left\langle \Delta\overline{\omega} \times \Delta\overline{\left.\frac{dq_s}{dp}\right|_{\theta^*}} \right\rangle \tag{4}$$

where Δ denotes change between two periods, <·> denotes mass-weighted vertical integration over the troposphere, overbar indicates a time average over the 1850 to 1900 baseline period or a projection period, g is the acceleration due to gravity, ω is the pressure velocity of vertical wind on the day of extreme precipitation, and $\frac{dq_s}{dp}|_{\theta^*}$ is the derivative of saturation specific humidity q_s at saturation equivalent potential temperature θ^*. We estimate the thermodynamic contribution $\Delta\overline{P}_{s\text{ther}}$ by replacing $\Delta\overline{\omega}$ with the 1850 to 1900 baseline mean vertical wind profile $\overline{\omega}$, that is, $\Delta\overline{P}_{s\text{ther}} = \frac{1}{g}\left\langle \Delta\overline{\omega} \times \Delta\overline{\left.\frac{dq_s}{dp}\right|_{\theta^*}} \right\rangle$, and represent the dynamic contribution by the remaining change $\Delta\overline{P}_{s\text{dyn}} = \Delta\overline{P_s} - \Delta\overline{P}_{s\text{ther}}$.

Note that all projected extreme precipitation changes are expressed as percentage changes relative to a baseline period (e.g., 1850 to 1900 or 1951 to 2020). Although evidence regarding how well climate models simulate relative changes in grid-cell extreme precipitation remains limited, it is suspected that models perform better in this regard than for absolute amount, particularly for the thermodynamic component (*74*). Detection and attribution studies have demonstrated that model simulated changes from anthropogenic forcings are detectable in precipitation extremes at station and grid-cell levels in many places around the world (*75*, *76*).

We also apply the decomposition to raw, unconstrained projections to elucidate the physical basis underlying the constrained level-of-global-warming approach for future changes in extreme precipitation. We examine intermodel correlations between the global warming during 1971 to 2020 and projected extreme precipitation changes as well as their thermodynamic contributions at individual grid cells. While the intermodel correlations for future grid-cell extreme precipitation changes are statistically significant over only about one-third of the global surface (e.g., fig. S18A for projected changes by 2071 to 2090 under the SSP5-8.5 emissions scenario), the thermodynamic contributions show strong and significant correlations across the vast majority of grid cells (fig. S18B), with a mean correlation coefficient of 0.7 over grid cells with significant correlations. Moreover, the projection error variance associated with the thermodynamic components of extreme precipitation changes constitutes a substantial fraction of the total

variance of the projected extreme precipitation changes, especially in extratropical regions (fig. S18, C and D). Collectively, these results provide a robust physical basis for the suggested strategy in mitigating uncertainties in future extreme precipitation projections arising from projected warming uncertainties.

Supplementary Materials

This PDF file includes:

Figs. S1 to S18

Tables S1 to S3

REFERENCES AND NOTES

1. V. Eyring, S. Bony, G. A. Meehl, C. A. Senior, B. Stevens, R. J. Stouffer, K. E. Taylor, Overview of the coupled model intercomparison project phase 6 (CMIP6) experimental design and organization. *Geosci. Model Dev.* **9**, 1937–1958 (2016).
2. S. C. Sherwood, M. J. Webb, J. D. Annan, K. C. Armour, P. M. Forster, J. C. Hargreaves, G. Hegerl, S. A. Klein, K. D. Marvel, E. J. Rohling, M. Watanabe, T. Andrews, P. Braconnot, C. S. Bretherton, G. L. Foster, Z. Hausfather, A. S. von der Heydt, R. Knutti, T. Mauritsen, J. R. Norris, C. Proistosescu, M. Rugenstein, G. A. Schmidt, K. B. Tokarska, M. D. Zelinka, An assessment of Earth's climate sensitivity using multiple lines of evidence. *Rev. Geophys.* **58**, e2019RG000678 (2020).
3. J. Zhu, C. J. Poulsen, B. L. Otto-Bliesner, High climate sensitivity in CMIP6 model not supported by paleoclimate. *Nat. Clim. Change* **10**, 378–379 (2020).
4. M. D. Zelinka, T. A. Myers, D. T. McCoy, S. Po-Chedley, P. M. Caldwell, P. Ceppi, S. A. Klein, K. E. Taylor, Causes of higher climate sensitivity in CMIP6 models. *Geophys. Res. Lett.* **47**, e2019GL085782 (2020).
5. M. Rugenstein, S. Dhame, D. Olonscheck, R. J. Wills, M. Watanabe, R. Seager, Connecting the SST pattern problem and the hot model problem. *Geophys. Res. Lett.* **50**, e2023GL105488 (2023).
6. Z. Hausfather, K. Marvel, G. A. Schmidt, J. W. Nielsen-Gammon, M. Zelinka, Climate simulations: Recognize the 'hot model' problem. *Nature* **605**, 26–29 (2022).
7. P. Voosen, 'Hot' climate models exaggerate Earth impacts. *Science* **376**, 685–685 (2022).
8. M. R. Asenjan, F. Brissette, J. Martel, R. Arsenault, Understanding the influence of "hot" models in climate impact studies: A hydrological perspective. *Hydrol. Earth Syst. Sci.* **27**, 4355–4367 (2023).
9. A. Cannon, The impact of "hot models" on a CMIP6 ensemble used by climate service providers in Canada: Do global constraints lead to appropriate differences in regional projections? *J. Clim.* **37**, 2141–2154 (2024).
10. R. Boyles, C. A. Nikiel, B. W. Miller, J. Littell, A. J. Terando, I. Rangwala, J. R. Alder, D. H. Rosendahl, A. M. Wootten, Approaches for using CMIP projections in climate model ensemble to address the 'hot model' problem. Open-File Report 2024–1008 (U.S. Geological Survey, 2024).
11. IPCC, Climate Change 2021: The Physical Science Basis. Contribution of Working Group I to the Sixth Assessment Report of the Intergovernmental Panel on Climate Change, V. Masson-Delmotte, P. Zhai, A. Pirani, S. L. Connors, C. Péan, S. Berger, N. Caud, Y. Chen, L. Goldfarb, M. I. Gomis, M. Huang, K. Leitzell, E. Lonnoy, J. B. R. Matthews, T. K. Maycock, T. Waterfield, O. Yelekçi, R. Yu, B. Zhou, Eds. (Cambridge Univ. Press, 2021).
12. K. B. Tokarska, M. B. Stolpe, S. Sippel, E. M. Fischer, C. J. Smith, F. Lehner, R. Knutti, Past warming trend constrains future warming in CMIP6 models. *Sci. Adv.* **6**, eaaz9549 (2020).
13. Y. Liang, N. P. Gillett, A. H. Monahan, Climate model projections of 21st century global warming constrained using the observed warming trend. *Geophys. Res. Lett.* **47**, e2019GL086757 (2020).
14. A. Ribes, S. Qasmi, N. P. Gillett, Making climate projections conditional on historical observations. *Sci. Adv.* **7**, eabc0671 (2021).
15. IPCC, Global Warming of 1.5°C. An IPCC Special Report on the impacts of global warming of 1.5°C above pre-industrial levels and related global greenhouse gas emission pathways, in the context of strengthening the global response to the threat of climate change, sustainable development, and efforts to eradicate poverty, V. Masson-Delmotte, P. Zhai, H.-O. Pörtner, D. Roberts, J. Skea, P. R. Shukla, A. Pirani, W. Moufouma-Okia, C. Péan, R. Pidcock, S. Connors, J. B. R. Matthews, Y. Chen, X. Zhou, M. I. Gomis, E. Lonnoy, T. Maycock, M. Tignor, T. Waterfield , Eds. (Cambridge Univ. Press, 2018).
16. K. W. Bowman, N. Cressie, X. Qu, A. Hall, A hierarchical statistical framework for emergent constraints: Application to snow-albedo feedback. *Geophys. Res. Lett.* **45**, 13050–13059 (2018).
17. T. G. Shepherd, Storyline approach to the construction of regional climate change information. *Proc. Math. Phys. Eng. Sci.* **475**, 20190013 (2019).
18. E. Baulenas, G. Versteeg, M. Terrado, J. Mindlin, D. Bojovic, Assembling the climate story: Use of storyline approaches in climate-related science. *Glob. Chall.* **7**, 2200183 (2023).
19. H. Shiogama, M. Watanabe, H. Kim, N. Hirota, Emergent constraints on future precipitation changes. *Nature* **602**, 612–616 (2022).
20. C. W. Thackeray, A. Hall, J. Norris, D. Chen, Constraining the increased frequency of global precipitation extremes under warming. *Nat. Clim. Change* **12**, 441–448 (2022).
21. C. Li, Q. Sun, J. Wang, Y. Liang, F. W. Zwiers, X. Zhang, L. Tong, Constraining projected changes in rare intense precipitation events across global land regions. *Geophys. Res. Lett.* **51**, e2023GL105605 (2024).
22. O. Linke, N. Feldl, J. Quass, Current-climate sea ice amount and seasonality as constraints for future Arctic amplification. *Environ. Res.: Climate* **2**, 045003 (2023).
23. Y.-H. Kim, S.-K. Min, N. P. Gillett, D. Notz, E. Malinina, Observationally-constrained projections of an ice-free Arctic even under a low emission scenario. *Nat. Commun.* **14**, 3139 (2023).
24. F. Lehner, A. W. Wood, J. A. Vano, D. M. Lawrence, M. P. Clark, J. S. Mankin, The potential to reduce uncertainty in regional runoff projections from climate models. *Nat. Clim. Chang* **9**, 926–933 (2019).
25. I. R. Simpson, K. A. McKinnon, F. V. Davenport, M. Tingley, F. Lehner, A. Fahad, D. Chen, Emergent constraints on the large-scale atmospheric circulation and regional hydroclimate: Do they still work in CMIP6 and how much can they actually constrain the future? *J. Clim.* **34**, 6355–6377 (2021).
26. X. Chen, T. Zhou, P. Wu, Z. Guo, M. Wang, Emergent constraints on future projections of the western North Pacific subtropical high. *Nat. Commun.* **11**, 2802 (2020).
27. I.-H. Park, S.-W. Yeh, S.-K. Min, S.-W. Son, Emergent constraints on future expansion of the Indo-Pacific warm pool. *Geophys. Res. Lett.* **49**, e2021GL097343 (2022).
28. E. Elbaum, C. I. Garfinkel, O. Adam, E. Morin, D. Rostkier-Edelstein, U. Dayan, Uncertainty in projected changes in precipitation minus evaporation: Dominant role of dynamic circulation changes and weak role for thermodynamic changes. *Geophys. Res. Lett.* **49**, e2022GL097725 (2022).
29. P. Dai, J. Nie, Y. Yu, R. Wu, Constraints on regional projections of mean and extreme precipitation under warming. *Proc. Natl. Acad. Sci. U.S.A.* **121**, e2312400121 (2024).
30. N. P. Gillett, Weighting climate model projections using observational constraints. *Philos. Trans. A Math. Phys. Eng. Sci.* **373**, 20140425 (2015).
31. E. C. Massoud, H. K. Lee, A. Terando, M. Wehner, Bayesian weighting of climate models based on climate sensitivity. *Commun. Earth Environ.* **4**, 365 (2023).
32. A. M. DeAngelis, X. Qu, M. D. Zelinka, A. Hall, An observational radiative constraint on hydrologic cycle intensification. *Nature* **528**, 249–253 (2015).
33. M. Watanabe, Y. Kamae, H. Shiogama, A. M. DeAngelis, K. Suzuki, Low clouds link equilibrium climate sensitivity to hydrological sensitivity. *Nat. Clim. Chang* **8**, 901–906 (2018).
34. H. Douville, Robust and perfectible constraints on human-induced Arctic amplification. *Commun. Earth Environ.* **4**, 283 (2023).
35. A. J. Cannon, Multivariate quantile mapping bias correction: An N-dimensional probability density function transform for climate model simulations of multiple variables. *Clim. Dyn.* **50**, 31–49 (2018).
36. S. Lange, Trend-preserving bias adjustment and statistical downscaling with ISIMIP3BASD (V1.0). *Geosci. Model Dev.* **12**, 3055–3070 (2019).
37. B. C. O'Neill, C. Tebaldi, D. P. van Vuuren, V. Eyring, P. Friedlingstein, G. Hurtt, R. Knutti, E. Kriegler, J.-F. Lamarque, J. Lowe, G. A. Meehl, R. Moss, K. Riahi, B. M. Sanderson, The scenario model intercomparison project (ScenarioMIP) for CMIP6. *Geosci. Model Dev.* **9**, 3461–3482 (2016).
38. X. Hu, J. Ma, J. Ying, M. Cai, Y. Kong, Inferring future warming in the Arctic from the observed global warming trend and CMIP6 simulations. *Adv. Clim. Chang. Res.* **12**, 499–507 (2021).
39. C. P. Morice, J. J. Kennedy, N. A. Rayner, J. P. Winn, E. Hogan, R. E. Killick, R. J. H. Dunn, T. J. Osborn, P. D. Jones, I. R. Simpson, An updated assessment of near-surface temperature change from 1850: The HadCRUT5 data set. *J. Geophys. Res. Atmos.* **126**, e2019JD032361 (2021).
40. E. M. Fischer, J. Sedláček, E. Hawkins, R. Knutti, Models agree on forced response pattern of precipitation and temperature extremes. *Geophy. Res. Lett.* **41**, 8554–8562 (2014).
41. C. Li, F. W. Zwiers, X. Zhang, G. Li, How much information is required to well constraint local estimates of future precipitation extremes? *Earths Future* **7**, 11–24 (2019).
42. C. Li, F. W. Zwiers, X. Zhang, G. Chen, J. Lu, G. Li, J. Norris, Y. Tan, Y. Sun, M. Liu, Larger increases in more extreme local precipitation events as climate warms. *Geophy. Res. Lett.* **46**, 6885–6891 (2019).
43. P. A. O'Gorman, T. Schneider, The physical basis for increases in precipitation extremes in simulations of 21st-century climate change. *Proc. Natl. Acad. Sci. U.S.A.* **106**, 14773–14777 (2009).
44. S. Pfahl, P. A. O'Gorman, E. M. Fischer, Understanding the regional pattern of projected future changes in extreme precipitation. *Nat. Clim. Change* **7**, 423–427 (2017).
45. Q. Sun, F. Zwiers, X. Zhang, Y. Tan, The effect of greenhouse gas-induced warming on the impact of El Niño and La Niña events on daily precipitation extremes in the boreal cold season. *J. Clim.* **36**, 6393–6407 (2023).

46. M. Iturbide, J. M. Gutiérrez, L. M. Alves, J. Bedia, R. Cerezo-Mota, E. Cimadevilla, A. S. Cofiño, A. D. Luca, S. H. Faria, I. V. Gorodetskaya, M. Hauser, S. Herrera, K. Hennessy, H. T. Hewitt, R. G. Jones, S. Krakovska, R. Manzanas, D. Martínez-Castro, G. T. Narisma, I. S. Nurhati, I. Pinto, S. I. Seneviratne, B. van den Hurk, C. S. Vera, An update of IPCC climate reference regions for subcontinental analysis of climate model data: Definition and aggregated datasets. *Earth Syst. Sci. Data* **12**, 2959–2970 (2020).
47. E. Hawkins, R. Sutton, Time of emergence of climate signals. *Geophys. Res. Lett.* **39**, L01702 (2012).
48. C. Mora, A. G. Frazier, R. J. Longman, R. S. Dacks, M. M. Walton, E. J. Tong, J. J. Sanchez, L. R. Kaiser, Y. O. Satender, J. M. Anderson, C. M. Ambrosino, I. Fernandez-Silva, L. M. Giuseffi, T. W. Giambelluca, The projected timing of climate departure from recent variability. *Nature* **502**, 183–187 (2013).
49. S. A. Henson, C. Beaulieu, T. Ilyina, J. G. John, M. Long, R. Séférian, J. Tjiputra, J. L. Sarmiento, Rapid emergence of climate change in environmental drivers of marine ecosystems. *Nat. Commun.* **8**, 14682 (2017).
50. Center for International Earth Science Information Network - CIESIN - Columbia University. Gridded Population of the World, Version 4 (GPWv4): Population Count, Revision 11. Palisades, NY: NASA Socioeconomic Data and Applications Center (SEDAC, 2018).
51. I. Mahlstein, R. Knutti, S. Solomon, R. W. Portmann, Early onset of significant local warming in low latitude countries. *Environ. Res. Lett.* **6**, 034009 (2011).
52. C. Li, Y. Fang, K. Caldeira, X. Zhang, N. S. Diffenbaugh, A. M. Michalak, Widespread persistent changes to temperature extremes occurred earlier than predicted. *Sci. Rep.* **8**, 1007 (2018).
53. A. D. King, M. G. Donat, E. M. Fischer, E. Hawkins, L. V. Alexander, D. J. Karoly, A. J. Dittus, S. C. Lewis, S. E. Perkins, The timing of anthropogenic emergence in simulated climate extremes. *Environ. Res. Lett.* **10**, 094015 (2015).
54. L. Warszawski, K. Frieler, V. Huber, F. Piontek, O. Serdeczny, J. Schewe, The Inter-sectoral Impact Model Intercomparison Project (ISI-MIP): Project framework. *Proc. Natl. Acad. Sci. U.S.A.* **111**, 3228–3232 (2013).
55. A. Orlov, J. Sillmann, K. Aunan, T. Kjellstrom, A. Aaheim, Economic costs of heat-induced reductions in worker productivity due to global warming. *Glob. Environ. Change* **63**, 102087 (2020).
56. P. Waidelich, F. Batibeniz, J. Rising, J. S. Kikstra, S. I. Seneviratne, Climate damage projections beyond annual temperature. *Nat. Clim. Change* **14**, 592–599 (2024).
57. D. Jiménez-de-la-Cuesta, T. Mauritsen, Emergent constraints on Earth's transient and equilibrium response to doubled CO_2 from post-1970s global warming. *Nat. Geosci.* **12**, 902–905 (2019).
58. Y. Liang, N. P. Gillett, A. H. Monahan, Emergent constraints on CMIP6 climate warming projections: Contrasting cloud- and surface temperature-based constraints. *J. Clim.* **35**, 1809–1824 (2022).
59. C. J. Smith, G. R. Harris, M. D. Palmer, N. Bellouin, W. Collins, G. Myhre, M. Schulz, J.-C. Golaz, M. Ringer, T. Storelvmo, P. M. Forster, Energy budget constraints on the time history of aerosol forcing and climate sensitivity. *J. Geophys. Res. Atmos.* **126**, e2020JD033622 (2021).
60. A. Ribes, S. Planton, L. Terray, Application of regularized optimal fingerprinting to attribution. Part I: Method, properties and idealized analysis. *Clim. Dyn.* **41**, 2817–2836 (2013).
61. C. Li, Z. Wang, F. W. Zwiers, X. Zhang, Improving the estimation of human climate influence by selecting appropriate forcing simulations. *Geophys. Res. Lett.* **48**, e2021GL095500 (2021).
62. Y. Dong, K. C. Armour, M. D. Zelinka, C. Proistosescu, D. S. Battisti, C. Zhou, T. Andrews, Intermodel spread in the pattern effect and its contribution to climate sensitivity in CMIP5 and CMIP6 models. *J. Clim.* **33**, 7755–7775 (2020).
63. C. Zhou, M. D. Zelinka, A. E. Dessler, M. Wang, Greater committed warming after accounting for the pattern effect. *Nat. Clim. Change* **11**, 132–136 (2021).
64. M. J. Alessi, M. A. A. Rugenstein, Surface temperature pattern scenarios suggest higher warming rates than current projections. *Geophys. Res. Lett.* **50**, e2023GL105795 (2023).
65. S. Zhang, P. Stier, G. Dagan, C. Zhou, M. Wang, Sea surface warming patterns drive hydrological sensitivity uncertainties. *Nat. Clim. Change* **13**, 545–553 (2023).
66. K. C. Armour, C. Proistosescu, Y. Dong, L. C. Hahn, E. Blanchard-Wrigglesworth, A. G. Pauling, R. C. J. Wills, T. Andrews, M. F. Stuecker, S. Po-Chedley, I. Mitevski, P. M. Forster, J. M. Gregory, Sea-surface temperature pattern effects have slowed global warming and biased warming-based constraints on climate sensitivity. *Proc. Natl. Acad. Sci. U.S.A.* **121**, e2312093121 (2024).
67. M. Watanabe, S. M. Kang, M. Collins, Y. Hwang, S. McGregor, M. F. Stuecker, Possible shift in controls of the tropical Pacific surface warming pattern. *Nature* **630**, 315–324 (2024).
68. Y. Liang, N. P. Gillett, A. H. Monahan, Accounting for Pacific climate variability increases projected global warming. *Nat. Clim. Change* **14**, 608–614 (2024).
69. B. Huang, M. J. Menne, T. Boyer, E. Freeman, B. E. Gleason, J. H. Lawrimore, C. Liu, J. J. Rennie, C. Schreck, F. Sun, R. S. Vose, C. N. Williams, X. Yin, H.-M. Zhang, Uncertainty estimates for sea surface temperature and land surface air temperature in NOAAGlobalTemp version 5. *J. Clim.* **33**, 1351–1379 (2020).
70. N. J. L. Lenssen, G. A. Schmidt, J. E. Hansen, M. J. Menne, A. Persin, R. Ruedy, D. Zyss, Improvements in the GISSTEMP uncertainty models. *J. Geophys. Res. Atmos.* **124**, 6307–6326 (2019).
71. W. Sun, Y. Yang, L. Cao, W. Dong, B. Huang, P. Jones, Q. Li, Description of the China global merged surface temperature version 2.0. *Earth Syst. Sci. Data* **14**, 1677–1693 (2022).
72. B. Huang, V. F. Banzon, E. Freeman, J. Lawrimore, W. Liu, T. C. Peterson, T. M. Smith, P. W. Thorne, S. D. Woodruff, H. Zhang, Extended reconstructed sea surface temperature version 4 (ERSST.v4). Part I: Upgrades and intercomparisons. *J. Clim.* **28**, 911–930 (2015).
73. N. P. Gillett, H. Shiogama, B. Funke, G. Hegerl, R. Knutti, K. Matthes, B. D. Santer, D. Stone, C. Tebaldi, The detection and attribution model intercomparison project (DAMIP v1.0) contribution to CMIP6. *Geosci. Model Dev.* **9**, 3685–3697 (2016).
74. E. M. Fischer, R. Knutti, Observed heavy precipitation increase confirms theory and early models. *Nat. Clim. Change* **6**, 986–991 (2016).
75. Q. Sun, F. Zwiers, Z. Zhang, J. Yan, Quantifying the human influence on the intensity of extreme 1- and 5-day precipitation amounts at global, continental, and regional scales. *J. Clim.* **35**, 195–210 (2022).
76. J. S. Nanditha, G. Villarini, H. Kim, P. Naveau, Strong linkage between observed daily precipitation extremes and anthropogenic emissions across the contiguous United States. *Geophys. Res. Lett.* **51**, e2024GL095553 (2024).

Acknowledgments: We thank the World Climate Research Programme's Working Group on Coupled Modeling and the individual modeling groups for their efforts in making CMIP data available. **Funding:** This work was supported by the National Key R&D Program of China (2020YFA0608901) and the National Natural Science Foundation of China (42075026). **Author contributions:** Conceptualization: C.L., F.W.Z., X.Z., and Y.L. Methodology: C.L., F.W.Z., X.Z., Y.L., and T.L. Software: C.L. and J.L. Validation: C.L., F.D., and Y.L. Formal analysis: C.L., F.D., J.L., and J.W. Investigation: C.L., F.D., J.L., Y.L., and T.L. Resources: C.L. Data curation: C.L., F.D., and J.L. Writing—original draft: C.L., F.W.Z., E.M.F., F.D., and J.W. Writing—review and editing: C.L., F.W.Z., X.Z., E.M.F., F.D., J.L., J.W., Y.L., T.L., and L.Y. Visualization: C.L., F.D., and L.Y. Supervision: C.L. and F.W.Z. Project administration: C.L. Funding acquisition: C.L. **Competing interests:** The authors declare that they have no competing interests. **Data and materials availability:** All data needed to evaluate the conclusions in the paper are present in the paper and/or the Supplementary Materials. The HadCRUT5 temperature observations are available at https://metoffice.gov.uk/hadobs/hadcrut5/. The Reconstructed Sea Surface Temperature version 5 dataset is available at https://ncei.noaa.gov/products/extended-reconstructed-sst. The CMIP6 climate model simulations are available at https://esgf-node.llnl.gov/search/cmip6/. The online interactive tool for the developed constraint method can be found at https://ecop-earth.com/.

Submitted 5 July 2024
Accepted 23 January 2025
Published 26 February 2025
10.1126/sciadv.adr5346